ISSN 1063-7737, Astronomy Letters, 2018, Vol. 44, No. 6, pp. 378–389. © Pleiades Publishing, Inc., 2018.
Original Russian Text © I.A. Mereminskiy, S.A. Grebenev, A.V. Prosvetov, A.N. Semena, 2018, published in Pis'ma v Astronomicheskii Zhurnal, 2018, Vol. 44, No. 6, pp. 413–425.

# Low-Frequency Quasi-Periodic Oscillations in the X-ray Nova MAXI J1535-571 at the Initial Stage of Its 2017 Outburst

**I. A. Mereminskiy*, S. A. Grebenev, A. V. Prosvetov, and A. N. Semena**

*Space Research Institute, Russian Academy of Sciences, Profsoyuznaya ul. 84/32, Moscow, 117997 Russia*

Received December 1, 2017

**Abstract**—We report the discovery of low-frequency quasi-periodic oscillations (QPOs) in the power spectrum of the X-ray nova MAXI J1535-571 at the initial stage of its outburst in September 2017. Based on data from the SWIFT and INTEGRAL instruments, we have traced the evolution of the QPO parameters (primarily their frequency) with time and their correlation with changes in the X-ray spectrum of the source (changes in the emission flux and hardness). We place constraints on the theoretical QPO generation models.

**DOI:** 10.1134/S106377371806004X

Keywords: *X-ray novae, black holes, disk accretion, X-ray emission, power spectra, low-frequency noise, quasi-periodic oscillations.*

## INTRODUCTION

The X-ray transient MAXI J1535-571 with a hard power-law emission spectrum was discovered on September 2, 2017, in the constellation Norma, $\sim 1^\circ$ away from the Galactic plane, simultaneously by the GSC/MAXI instrument (Negoro et al. 2017) and the BAT/SWIFT monitor (Markwardt et al. 2017). The promptly performed observations by the XRT and UVOT telescopes of the SWIFT observatory allowed the source to be localized with an accuracy up to 1.″5 (Kennea et al. 2017) and then its optical counterpart to be found (Scaringi et al. 2017). The source was detected in the radio (Russell et al. 2017) and near-infrared (Dincer 2017) bands as well as at millimeter wavelengths (Tetarenko et al. 2017). An additional confirmation that the optical object is actually the counterpart of the X-ray one was the presence of the Br$\gamma$ hydrogen line (Britt et al. 2017) in its infrared spectrum, which is associated with accretion processes (Bandyopadhyay et al. 1997). One week after the discovery of the source, Nakahira et al. (2017) and Kennea (2017) reported a softening of its X-ray spectrum.

Such a behavior is typical for X-ray novae, i.e., low-mass X-ray binaries in which there is nonstationary accretion onto a black hole (or a neutron star with a weak magnetic field). It is common practice to describe the development of the outbursts of such binaries in terms of the change of their "states" caused by a change in the regime of accretion. During each state the X-ray nova emission has its unique spectral and timing properties (see, e.g., Sunyaev et al. 1988, 1991; Grebenev et al. 1993, 1997; Tanaka and Shibazaki 1996; Remillard and McClintock 2006; Belloni et al. 2010; Cherepashchuk 2013).

All outbursts of X-ray novae begin with a low (hard) state in which the central, hot, optically thin accretion disk region puffed up by instabilities makes a major contribution to the radiation. The observed power-law spectrum with an exponential cutoff at high energies is formed in this region by Comptonization of the radiation on high-temperature electrons. As the luminosity (accretion rate) increases, the hard state changes into an intermediate hard one, then an intermediate soft one, and, finally, a high (soft) state. The radiation from the outer cold, optically thick accretion disk begins to dominate in the source's spectrum. The transition between the states suggests that the size of the inner high-temperature region decreases with increasing accretion rate. At such an accretion rate the outer disk becomes too dense and its evaporation begins later, closer to the black hole, in the region of maximum energy release.

Measuring the radius of the inner region (or the blackbody disk truncation radius) $r_{\rm tr}$ at different outburst stages is critical for testing this picture. However, the results of such measurements are so far contradictory—an analysis of the blackbody component in the spectrum of X-ray novae shows that in a number of systems the cold accretion disks with $kT_{\rm br} \sim 0.1-0.5$ keV probably reach the

*E-mail: i.a.mereminskiy@gmail.com

innermost stable circular orbit near the black hole (Miller et al. 2006a, 2006b; Reis et al. 2011), while an analysis of the hard X-ray component reflected from the cold disk and, in particular, the relativistically broadened 6.4 keV neutral iron line leads to large truncation radii in some cases (Fürst et al. 2015) and to small ones in other cases (Miller et al. 2015).

The different states of X-ray novae differ not only by the spectral shape but also by the pattern of their rapid flux variability (Grebenev et al. 1993; Belloni 2010). In the low (hard) state the X-ray power spectrum usually includes a broad frequency-limited ("red–white") noise component on which one or more narrow Lorentzian peaks with frequencies $f_{\rm QPO}$ from $\sim$0.1 to several Hz indicative of low-frequency quasi-periodic oscillations of the flux (LF QPOs) are superimposed. Such LF QPOs were first described by Ebisawa et al. (1989) and Grebenev et al. (1991). The red–white noise can be successfully fitted by a King function. It has been established that the break frequency $f_{\rm br}$ above which the noise amplitude begins to rapidly decrease is related by a linear relation to the fundamental QPO frequency $f_{\rm QPO}$ (Wijnands and van der Klis 1999; see also Prosvetov and Grebenev 2015), with this relation also holding for both systems with black holes and systems with neutron stars.

The origin of LF QPOs has not yet been established, despite the numerous attempts to do this (see, e.g., Vikhlinin et al. 1994; Stella and Vietri 1998; Titarchuk et al. 2007; Ingram et al. 2009). It is important that in some QPO models, for example, relativistic disk precession (Stella and Vietri 1998) or diffusive propagation of perturbations in the disk (Titarchuk et al. 2007), the frequency $f_{\rm QPO}$ directly depends on the truncation radius of the accretion disk $r_{\rm tr}$, which allows the change in this radius (the size of the high-temperature central zone) during the outburst to be traced.

Such LF QPOs with a gradually changing frequency were detected in the X-ray power spectrum of MAXI J1535-571 on September 11, 2017, eight days after its discovery (Mereminskiy and Grebenev 2017). This paper is devoted to their detailed analysis.

## DATA ANALYSIS

After the discovery of MAXI J1535-571, its observations were begun at many of the then operating X-ray telescopes. In this paper we use the observations of this source by the IBIS/ISGRI (Lebrun et al. 2003; Ubertini et al. 2003) and JEM-X (Lund et al. 2003) telescopes of the INTEGRAL observatory (Winkler et al. 2003), the BAT (Barthelmy et al. 2005) and XRT (Burrows et al. 2005) telescopes of the SWIFT observatory (Gehrels et al. 2004), and the GCS monitor (Mihara et al. 2011) of the MAXI observatory (Matsuoka et al. 2009).

The list of observations of the source by the INTEGRAL and SWIFT instruments used in the paper is given in Table 1. Note that a powerful solar flare occurred at the beginning of revolution 1861 of the INTEGRAL satellite (MJD 58 007.3-58 009.4), as a result of which the observations planned for this revolution were interrupted.

### *Investigation of the Variability*

We were interested primarily in the rapid variability of the source. The XRT/SWIFT data obtained in the fast timing mode were passed through the standard pipeline `xrtpipeline` and then barycentered. Because of the source's brightness, the telescope performed most of the observations in the regime of "overloading." In this case, the photon arrival frequency exceeded the detector array sampling frequency. If several photons fell on the sampled detector area between readouts, then they either were recorded as one higher-energy photon or were ignored altogether, because their total energy exceeded the specified threshold. When analyzing the temporal variability in this regime, we, however, did not resort to a standard practice, i.e., the exclusion of detector areas with an excessively large count rate. Overloading affects primarily the measured energy spectrum of the source and has no significant influence on the QPO frequency, whose measurement was our most important task. We made sure of this in several observations by excluding five most illuminated detector array columns in each of them. For our analysis we used the light curves with a resolution of 20 ms in the energy range 0.8–10 keV.

The data from the JEM-X and IBIS/ISGRI telescopes of the INTEGRAL observatory were processed with the standard data analysis package OSA-10.1 and barycentered. We used the light curves with a resolution of 0.1 s in the energy ranges 3–20 and 20–200 keV, respectively. Several X-ray sources fell within the fields of view of the telescopes at once. Although we used the detector pixel illumination fraction (PIF) by photons from the source MAXI J1535-571 of interest when constructing its light curves, the photons from other sources also made a certain contribution. Fortunately, MAXI J1535-571 was much brighter than other objects and the distortions introduced by them were insignificant.

**Table 1.** Observations and parameters of the LF QPOs in MAXI J1535-571

| Instrument[a] | Observation | Beginning | End | QPO | | 1H[b] |
|---|---|---|---|---|---|---|
| | ID | MJD-58 000.00 | | frequency[c] | width[d] | |
| XRT + BAT | 10264003 | 4.28 | 4.36 | $0.21 \pm 0.03$ | $0.22 \pm 0.07$ | *[e] |
| IBIS | 18600002-06 | 4.53 | 4.75 | $0.23 \pm 0.01$ | $0.14 \pm 0.06$ | |
| BAT[f] | 39407002 | 4.63 | 4.93 | $0.24 \pm 0.01$ | $0.14 \pm 0.06$ | |
| IBIS | 18600007-11 | 4.75 | 4.96 | $0.24 \pm 0.01$ | $0.14 \pm 0.04$ | |
| IBIS | 18600012-16 | 4.96 | 5.18 | $0.28 \pm 0.02$ | $0.16 \pm 0.08$ | |
| IBIS | 18600017-21 | 5.18 | 5.39 | $0.37 \pm 0.01$ | $0.11 \pm 0.04$ | |
| BAT[f] | 87473001 | 5.28 | 5.45 | $0.37 \pm 0.01$ | $0.11 \pm 0.04$ | |
| IBIS | 18600022-26 | 5.39 | 5.63 | $0.45 \pm 0.01$ | $0.15 \pm 0.04$ | |
| IBIS | 18600027-31 | 5.63 | 5.88 | $0.53 \pm 0.01$ | $0.11 \pm 0.03$ | |
| IBIS | 18600032-37 | 5.89 | 6.14 | $0.68 \pm 0.02$ | $0.19 \pm 0.05$ | |
| IBIS | 18600038-42 | 6.14 | 6.36 | $0.89 \pm 0.02$ | $0.16 \pm 0.04$ | |
| IBIS | 18600043-47 | 6.36 | 6.57 | $1.03 \pm 0.01$ | $0.13 \pm 0.03$ | |
| BAT[f] | 30806051 | 6.27 | 6.95 | $1.03 \pm 0.01$ | $0.13 \pm 0.03$ | |
| XRT + BAT | 10264004 | 7.27 | 7.29 | $1.87 \pm 0.03$ | $0.21 \pm 0.05$ | * |
| XRT | 10264005 | 8.26 | 8.27 | $2.15 \pm 0.02$ | $0.10 \pm 0.03$ | * |
| XRT + BAT | 10264007 | 9.01 | 9.02 | $2.67 \pm 0.03$ | $0.26 \pm 0.09$ | |
| JEM-X | 18620019 | 10.54 | 10.58 | $1.98 \pm 0.05$ | $0.11 \pm 0.10$ | |
| XRT + BAT | 10264006 | 10.93 | 10.94 | $2.22 \pm 0.03$ | $0.20 \pm 0.05$ | * |
| JEM-X | 18620034 | 11.19 | 11.23 | $2.11 \pm 0.06$ | $0.21 \pm 0.10$ | |
| XRT + BAT | 10264008 | 11.39 | 11.40 | $2.32 \pm 0.03$ | $0.24 \pm 0.08$ | * |
| XRT + BAT | 10264009 | 12.12 | 12.13 | $2.29 \pm 0.02$ | $0.19 \pm 0.06$ | * |
| XRT | 88245001 | 13.18 | 13.20 | $2.59 \pm 0.02$ | $0.24 \pm 0.05$ | * |
| XRT | 88245001 | 13.24 | 13.25 | $2.89 \pm 0.06$ | $0.32 \pm 0.18$ | |
| JEM-X | 18630034 | 13.89 | 13.92 | $2.64 \pm 0.04$ | $0.28 \pm 0.11$ | |
| XRT + BAT | 10264010 | 14.18 | 14.19 | $3.22 \pm 0.04$ | $0.29 \pm 0.07$ | * |
| XRT | 88245002 | 16.97 | 16.98 | – | | |

[a] The XRT and BAT telescopes of the SWIFT observatory and the JEM-X and IBIS/ISGRI of the INTEGRAL observatory.
[b] The presence of the first harmonic of the QPO peak in the power spectrum.
[c] The frequency of the Lorentzian peak, Hz.
[d] The width of the Lorentzian peak, Hz; it depends on energy and, therefore, the peak is narrower in the IBIS spectrum.
[e] In this spectrum the first harmonic at $f_{1H} = 0.42 \pm 0.02$ Hz is noticeably more significant than the fundamental one.
[f] BAT was used only for the spectral measurements, the QPO frequency was determined from the simultaneous IBIS observations.

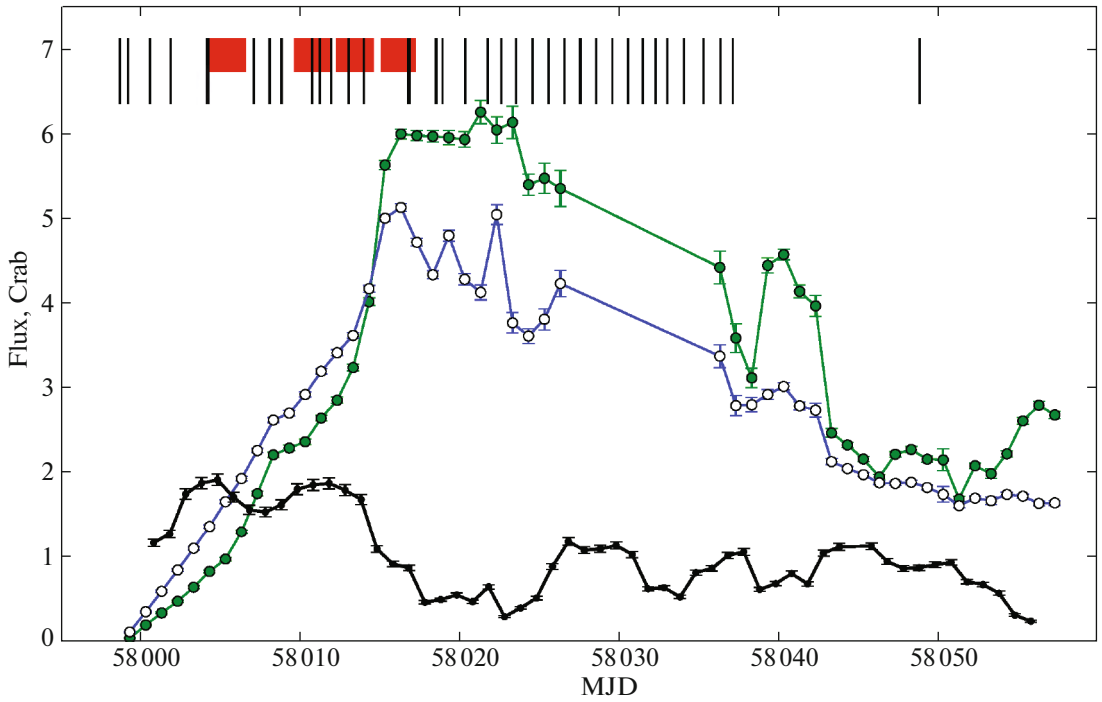


**Fig. 1.** (Color online) Light curves of the X-ray nova MAXI J1535-571. The black small circles indicate the 15–50 keV flux from the BAT/SWIFT data, the green and blue (filled and open) large circles indicate the 2–4 and 4–10 keV fluxes from the MAXI data. MJD 58 000.00 corresponds to September 4, 2017. The red broad lines and black narrow lines at the top specify the intervals of INTEGRAL and XRT/SWIFT observations, respectively.

### *Investigation of the Radiation Spectra*

The evolution of the source's radiation spectrum during its outburst is also of interest. To obtain broadband (2–150 keV) spectra, we used the quasi-simultaneous MAXI and BAT/SWIFT observations. We took the parts of the spectra in the energy range 2–20 keV from the web page of the MAXI monitor (`http://maxi.riken.jp/mxondem`) and the parts of the spectra in the harder energy range 20–150 keV from the BAT/SWIFT observations in the survey mode. We used the histograms of detector events accumulated during the sky survey with a typical exposure time of 0.5–1.5 ks. Since such data are analyzed quite rarely, we described in detail the spectrum extraction procedure in the Appendix.

## RESULTS

### *Light Curves and the Transition to the Soft State*

Figure 1 presents the source's light curves during its outburst in the soft (2–4 and 4–10 keV, from the MAXI data) and hard (15–50 keV, from the BAT/SWIFT data) X-ray bands. The rising phase lasted for approximately 16 days (until MJD 58 015) in the soft X-ray band and was much shorter (about 5 days) in the hard one. Near MJD 58 015 the hard X-ray flux dropped sharply (on a time scale of 2 days) by a factor of ∼3, while the soft one rose by a factor of ∼2, with the 2–4 keV flux having exceeded the 4–10 keV flux for the first time. At this moment the spectral state of the source changed from hard to soft. It remained such at least for the next one and a half months, despite the fact that, as follows from the figure, the soft X-ray flux began to gradually decrease after ∼10 days of relative stability and reached the level observed in the hard state by the end of the observations.

Simultaneously with the transition of the source to the soft spectral state, the shape of its X-ray power spectrum also changed. Figure 2 presents the power spectra obtained during the XRT/SWIFT observations of the source at MJD 58 014 and 58 017 (ObsID 10264010 and 88245002, respectively). The first spectrum has a shape with pronounced powerful low-frequency noise (LFN) and two QPO peaks typical for the hard state, while the second spectrum is virtually indistinguishable from a flat "white" noise spectrum and does not contain any features, which is typical for the soft state of X-ray novae. In the energy range 0.8–10 keV the power of LFN (in the frequency range 0.1–10 Hz) and the fundamental QPO peak was ≃2 and 4% of the photon flux in the source's hard state and in total less than 2.7% in its soft state (90% confidence interval). Note that the feature in the light curves near MJD 58 008 resembling the

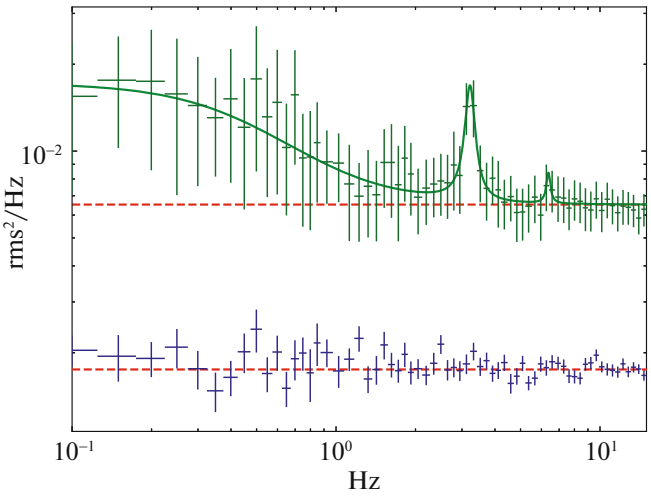


**Fig. 2.** (Color online) XRT/SWIFT power spectra for MAXI J1535-571 in the energy range 0.8–10 keV. The upper (green dots, the spectrum was multiplied by 4 for clarity) and lower (blue dots) spectra represent, respectively, the observations MJD 58 014, before the transition to the soft state, and MJD 58 017, after the transition. Low-frequency broadband noise and two QPO peaks corresponding to the fundamental frequency and the first harmonic are clearly seen in the power spectrum before the transition. There is virtually no noise in the power spectrum after the transition.

previous, failed attempt of the transition to the soft state was also accompanied by pronounced changes in the source's power spectrum.

As has already been said, this paper is devoted to investigating the quasi-periodic oscillations of the flux from the source. Therefore, below we will restrict our analysis to the initial outburst stage, i.e., before the source's transition to the soft (high) state.

### *Quasi-Periodic Oscillations*

We analyzed all the accessible XRT/SWIFT observations of the source performed in the timing mode. If an observation included several exposures separated by long interruptions, then the time intervals corresponding to them were considered separately. The power spectrum of each observation was fitted by a combination of the King function describing the broadband noise, one or two Lorentzians describing the QPOs, and the constant responsible for the Poisson noise power. Examples of our power spectra and their best fits by the adopted model at different outburst stages are shown in Fig. 3. The measured frequencies and widths of the fundamental QPO peak are given in Table 1. The asterisks mark the observations in which the first harmonic of the QPO peak was recorded. Curiously, during the first XRT/SWIFT observation of the source (MJD 58 004.3) the first harmonic in the power spectrum was brighter and appreciably more significant than the fundamental QPO peak.

We also used data from the IBIS/ISGRI and JEM-X telescopes of the INTEGRAL observatory in searching for QPOs. The contribution of the source to the total photon count rate by coded-aperture telescopes is appreciably smaller than its contribution to the count rate by focusing telescopes. Therefore, the low-frequency noise amplitude and the overall shape of the power spectrum for the source measured by these telescopes differ from those measured by XRT. The energy ranges in which the XRT and IBIS/ISGRI measurements were performed also differ. Nevertheless, the QPO peak in the power spectra obtained by the INTEGRAL telescopes is clearly seen, while the QPO frequency was measured by these telescopes with a high accuracy owing to the long exposures ($\gtrsim$15 ks). The results of these measurements are also included in Table 1. Because of the harder X-ray band, the QPO peak in these spectra is appreciably narrower than that in the XRT/SWIFT power spectra.

As has already been mentioned, after revolution 1860 the INTEGRAL observations were interrupted due to a solar flare, the instruments were activated, and the background of charged particles remained high for a long time after the resumption of their operation. Besides, the hard X-ray flux from the source dropped by almost a factor of 2 by this time and, therefore, the significance of the QPO detection by the IBIS/ISGRI telescope decreased dramatically. However, the QPO peak remained clearly seen in the power spectra measured by the JEM-X telescope in revolutions 1862–1863 (MJD 58 009.3–58 015.3), because the soft X-ray flux from the source rose dramatically. This allowed the XRT/SWIFT measurements of the QPO frequency to be supplemented at a late stage of the observing period under discussion.

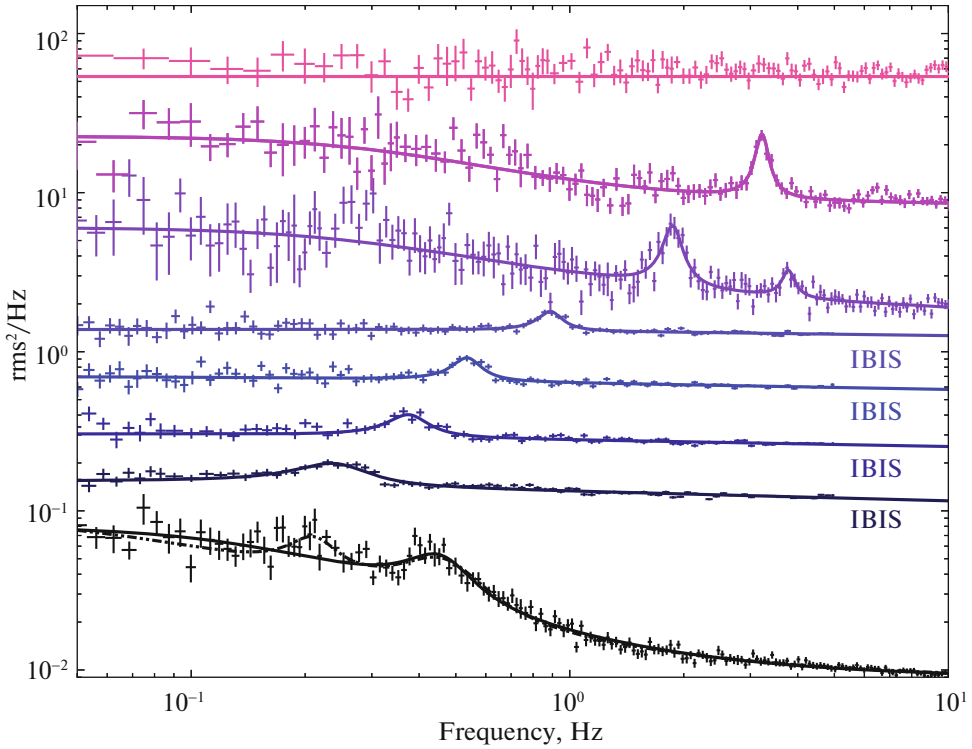


**Fig. 3.** (Color online) Evolution of the X-ray power spectrum and QPO peak (peaks) for MAXI J1535-571 from the XRT/SWIFT and IBIS/ISGRI/INTEGRAL data in the period MJD 58 004–58 017. The spectra in observations 10264003, 1860002-06, 18600017-21, 18600027-31, 18600038-42, 10264004, and 88245002, which are normalized to some factor for clarity, are shown from bottom to top. The solid lines indicate the best fits to the spectra by the adopted model (see the text). In the early spectrum the fundamental peak is indicated by the dashed line, because its significance is much lower than that of the first harmonic. The shift of the QPO peak toward higher frequencies from $f_{\rm QPO} \sim 0.23$–$3.22$ Hz and then its disappearance in observation MJD 58 017, after the source's transition to the soft state, are clearly seen.

Figure 4 shows how the QPO frequency changed during the outburst. Within the first hours of observations (MJD 58 004.3–58 005.0) the QPO frequency was ∼0.23 Hz, but then it began to monotonically increase. Between MJD 58 009.02 and MJD 58 010.56, at the instant the break was observed in the light curves of the X-ray nova, there was a reverse jump by ∼0.7 Hz in the QPO frequency, after which the frequency continued to increase, but more slowly. The filled circles in Fig. 4 indicate the evolution of the spectral softness $S$ in the standard X-ray band (the ratio of the fluxes in the 2–4 and 4–10 keV subbands). It remarkably correlates with the change in the QPO frequency. Obviously, this parameter reflects mainly the changes occurring in the blackbody radiation from the accretion disk.[1] Unfortunately, the available data do not allow us to perform real spectral measurements of the source's radiation in this band and to trace the evolution of the parameters of the blackbody spectral component (its temperature and truncation radius) in more detail.

It is also natural to investigate the dependence of the QPO frequency on the photon index of the hard part of the source's radiation spectrum, in particular, to check whether a characteristic saturation of the photon index is observed as the QPO frequency increases (see, e.g., Sobczak et al. 2000, Vignarca et al. 2003). For this purpose, we used the broadband MAXI + BAT/SWIFT spectra that were fitted in the energy range 5–150 keV by an absorbed power law with an exponential cutoff (`const*phabs*cutoffpl`). The hydrogen absorption column density was fixed at $N_{\rm H} = 4 \times 10^{22}$ cm$^{-2}$; the cross-calibration constant of the instruments in all cases differed from unity by no more than 15%. Unfortunately, the short exposure of the BAT/SWIFT observations does not allow the exponential cutoff energies to be measured accurately (the typical error is ≃15 keV for 40–60 keV) and, therefore, $E_{\rm cut}$ was fixed at a mean value of 50 keV. The energy range 2–5 keV was disregarded, because the component associated with the blackbody disk

[1] The spectral measurements performed in this period by the NuSTAR observatory (Xu et al. 2017) show that the contribution from the photons of the blackbody component to the spectrum at energies $\gtrsim$4 keV drops sharply. Nevertheless, the change in the QPO frequency turned out to correlate with the change in the 2–4 keV flux more poorly than with this spectral softness.

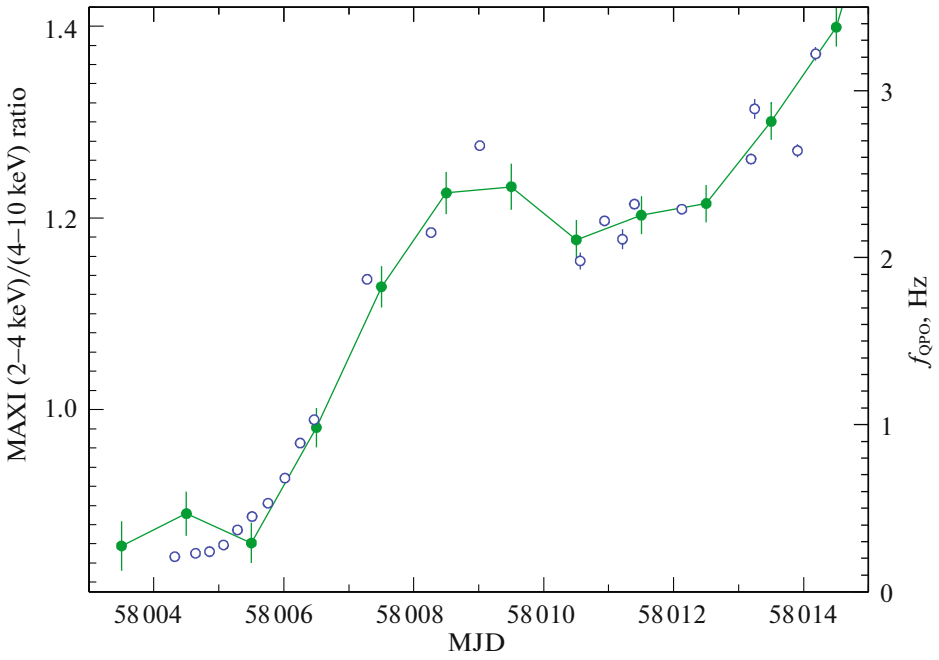


**Fig. 4.** (Color online) Evolution of the QPO frequency during the rising phase of the outburst from the data of Table 1 (open (blue) circles). The filled (green) circles connected by the solid line indicate the change in the source's X-ray softness (the ratio of the fluxes in the 2–4 and 4–20 keV subbands from the MAXI data).

radiation contributed noticeably to it. The changes in photon index are presented in Table 2 and indicated in Fig. 5 by the filled (green) circles. A gradual saturation of the photon index near $\alpha \sim 2.35$ as the QPO frequency increases above ~2 Hz seems to be actually present. The open (blue) circles in the same figure indicate the drop in flux in the energy range 5–100 keV.

## DISCUSSION

We traced the evolution of the low-frequency QPO parameters in the power spectrum of a new black hole candidate, the X-ray nova MAXI J1535-571, during its outburst in September 2017, at the rising phase, when it was in the hard spectral state. Using data from three X-ray telescopes, we traced the increase in the QPO frequency from ~0.2 to ~3 Hz for ~10 days, until the source's transition to the high soft state, and investigated the correlation of the QPO frequency with the X-ray spectral hardness.

The nature of QPOs has not yet been established. In some models for the origin of QPOs (see, e.g., Titarchuk et al. 2007) their frequency is determined by the Keplerian rotation frequency of the material in the accretion disk at its truncation radius, i.e., the boundary of the inner high-temperature region responsible for the observed hard X-ray radiation. Indeed, the appearance of periodic perturbations that are subsequently enhanced in the radiation-dominated plasma of the inner zone might be expected in this disk region. From the data in Fig. 4 we can then estimate the disk truncation radius $R_{\rm tr} = (\sqrt{2} f_{\rm QPO} R_{\rm g}/c)^{-2/3} R_{\rm g}$ and trace its change with time. Here, $R_{\rm g} = 2GM/c^2$ is the gravitational radius of a black hole. The result of such a calculation by assuming the black hole mass to be $M = 10\ M_\odot$ is indicated in Fig. 6a by the open (blue) circles. The behavior of the truncation radius is characterized by a rapid decrease from $\sim 10^3\ R_{\rm g}$ to $\sim 200\ R_{\rm g}$ within the first three days after MJD 58 005, a succeeding five-day period of relative stability, and a very slow further decrease to $\sim 160\ R_{\rm g}$ in the last two days.

The behavior of the truncation radius can be estimated independently from the law of change in spectral softness $S$ presented in Fig. 4 by taking into account the surprising correlation of this parameter with the QPO frequency and by assuming its proportionality to the surface temperature of the blackbody disk near its inner edge. According to Shakura and Sunyaev (1973), the dependence of this temperature on $R_{\rm tr}$ is given by the expression $\sigma T_{\rm tr}^4 = (3/8\pi)\ GM\dot{M}/R_{\rm tr}^3$, where $\dot{M}$ is the accretion rate and $\sigma$ is the Boltzmann constant; thus, $R_{\rm tr} \sim T_{\rm tr}^{-4/3}$. Accordingly, we attempted to fit the truncation radius

**Table 2.** Parameters of the integral X-ray spectrum of MAXI J1535-571[a]

| Observation | Beginning | End | QPO frequency[b] | Photon index, $\alpha$[c] | Flux[d] |
|---|---|---|---|---|---|
| SWIFT ObsID | MJD-58 000.00 | | | | |
| 10264003 | 4.28 | 4.36 | $0.42 \pm 0.02$ | $1.79 \pm 0.03$ | $2.3 \pm 0.1$ |
| 39407002 | 4.63 | 4.93 | $0.24 \pm 0.01$ | $1.83 \pm 0.04$ | $2.4 \pm 0.1$ |
| 87473001 | 5.28 | 5.45 | $0.37 \pm 0.01$ | $1.90 \pm 0.03$ | $2.2 \pm 0.1$ |
| 30806051 | 6.27 | 6.95 | $1.03 \pm 0.01$ | $2.07 \pm 0.03$ | $1.9 \pm 0.1$ |
| 10264004 | 7.27 | 7.29 | $1.87 \pm 0.03$ | $2.21 \pm 0.07$ | $1.5 \pm 0.1$ |
| 10264007 | 9.01 | 9.02 | $2.67 \pm 0.03$ | $2.30 \pm 0.07$ | $1.5 \pm 0.1$ |
| 10264006 | 10.93 | 10.94 | $2.22 \pm 0.03$ | $2.36 \pm 0.07$ | $1.7 \pm 0.1$ |
| 10264008 | 11.39 | 11.40 | $2.32 \pm 0.03$ | $2.33 \pm 0.07$ | $1.7 \pm 0.1$ |
| 10264009 | 12.12 | 12.13 | $2.29 \pm 0.02$ | $2.30 \pm 0.06$ | $1.7 \pm 0.1$ |
| 10264010 | 14.18 | 14.19 | $3.22 \pm 0.04$ | $2.40 \pm 0.07$ | $1.6 \pm 0.1$ |

[a] The best fit to the spectrum in the energy range 5–150 keV from the GSC/MAXI and BAT/SWIFT data.
[b] The QPO frequency determined from the XRT/SWIFT or IBIS/ISGRI/INTEGRAL data, Hz.
[c] The photon index in the energy range 5–100 keV.
[d] The 5–100 keV flux, $10^{-8}$ erg s$^{-1}$ cm$^{-2}$.

by the formula $R_{\rm tr} = A(S - S_0)^{-4/3}\ R_{\rm g}$. The best agreement was achieved at $A = 108 \pm 2$ and $S_0 = 0.60 \pm 0.01$. The best fit is indicated in Fig. 6a by the filled (green) circles. The two estimates agree well between themselves at $R_{\rm tr} \lesssim 600\ R_{\rm g}$. At larger truncation radii the disk temperature is apparently too low to be adequately described by the parameter $S$ determined at $h\nu > 2$ keV.

On the other hand, interesting estimates of the parameters of the inner hot disk zone can be obtained from the spectral variability of the hard X-ray radiation. For example, by considering the inner hot disk zone as a quasi-spherical one and by assuming that its electron temperature $kT_{\rm e} \simeq 50$ keV does not depend on the radius, we can use the well-known formulas of the Comptonization theory (Sunyaev and Titarchuk 1980) for the photon index forming in the emission cloud:

$$\alpha = -\frac{1}{2} + \sqrt{\frac{9}{4} + \gamma},$$

where $\gamma = (\pi^2/3)(\tau_{\rm T} + 2/3)^{-2}\ (m_{\rm e}c^2/kT_{\rm e})$, and estimate the Thomson optical depth of the cloud (see Fig. 6b). In this figure the optical depth $\tau_{\rm T}$ is presented as a function of the radius of the inner zone $R_{\rm tr}$, which we found by again assuming that the QPOs forming here have a Keplerian frequency. The optical depth $\tau_{\rm T}$ changes from $\sim$2.7 to $\sim$1.5, in agreement with our assumptions. We see that $\tau_{\rm T}$ and $R_{\rm tr}$ correlate well (unambiguously) between themselves. We fitted this dependence by the formula $\tau_{\rm T} = (R_{\rm tr}/R_* + B)^{\beta}$. The best agreement was achieved at $B = 1.8 \pm 0.1$, $R_* = (40 \pm 2)R_{\rm g}$, and $\beta = 0.3 \pm 0.01$; the best fit is indicated in Fig. 6b by the solid line. The solid curve in Fig. 5 indicates the result of using this formula to estimate the photon index $\alpha$ within the Comptonization theory. We see good agreement of this curve with the results of direct $\alpha$ measurements.

This formula describes the observed drop in the hard (Comptonized) X-ray flux from the source in this period equally well. If the radiation originates in the quasi-spherical cloud of an optically semitransparent plasma, then its flux at other constant cloud parameters must be directly proportional to its Thomson optical depth (Sunyaev and Titarchuk 1980). Indeed, our attempt to fit the drop in flux indicated in Fig. 5 by the open (blue) circles by the formula $F = D\tau_{\rm T}$ turned out to be successful—the result for the best value of the parameter $D = 0.88 \pm 0.01$ is indicated in this figure by the dashed (blue) line.

On the whole, it can be said that the assumption that the QPO frequency is equal to the Kep-

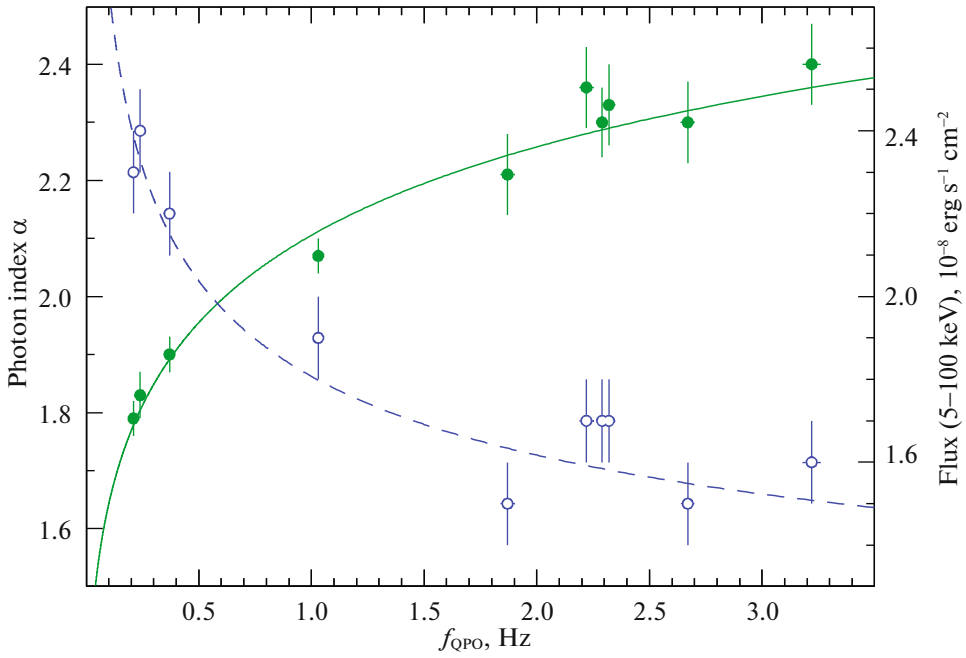


**Fig. 5.** (Color online) Photon index $\alpha$ (filled circles) and flux (open circles) of the broadband (5–150 keV, the MAXI and BAT/SWIFT data) X-ray spectrum for MAXI J1535-571 versus QPO frequency (measured by the XRT/SWIFT and IBIS/ISGRI/INTEGRAL telescopes). The curves indicate the best fits described in the Section Discussion.

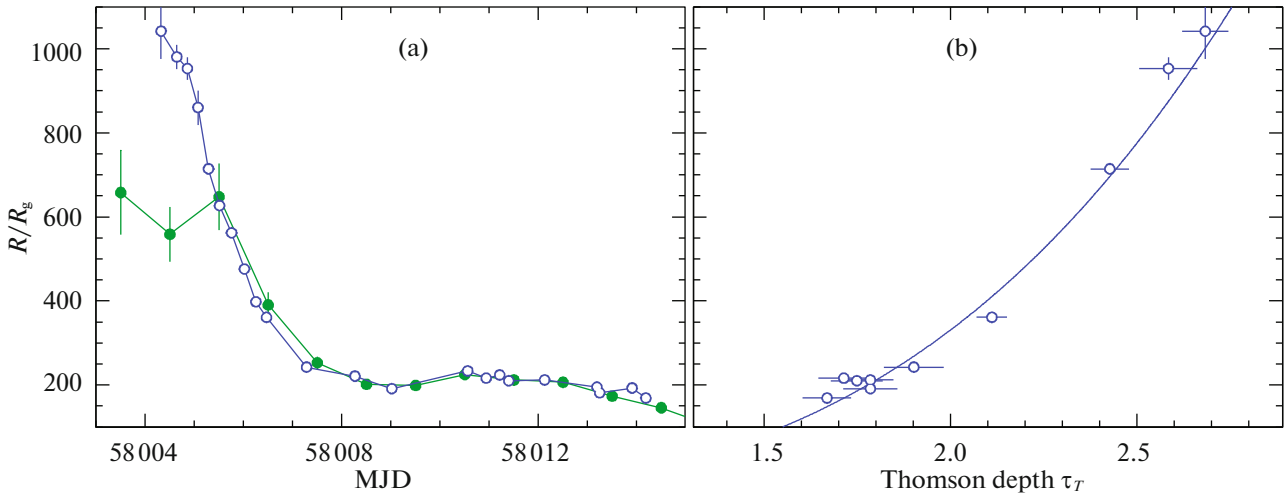


**Fig. 6.** (Color online) (a) Change in the truncation radius of the blackbody accretion disk in the X-ray nova MAXI J1535-571 with time at the initial outburst stage. It was determined from the observed evolution of the LF QPO frequency in the power spectrum of the source (blue open circles) and the evolution of its X-ray spectral softness (filled green circles). (b) Dependence of the Thomson depth of the central high-temperature accretion disk zone in the source on its radius (blackbody disk truncation radius). It was determined from the change in the photon index of the hard X-ray radiation.

lerian frequency at some radius comparable to the truncation radius of the blackbody accretion disk in MAXI J1535-571 leads to self-consistent and reasonable results. However, this contradicts the results from Xu et al. (2017) of a spectral analysis of the NuSTAR data obtained during the source's observation almost simultaneously with our first detection of QPOs (at a frequency of ~0.21 Hz in the interval MJD 58 004.28-58 004.36). The authors obtained stringent constraints on the black hole spin ($a > 0.84$) and the disk truncation radius ($R_{tr} < 2.01 R_{ISCO} \simeq 2.7\ R_g$). At such a truncation radius

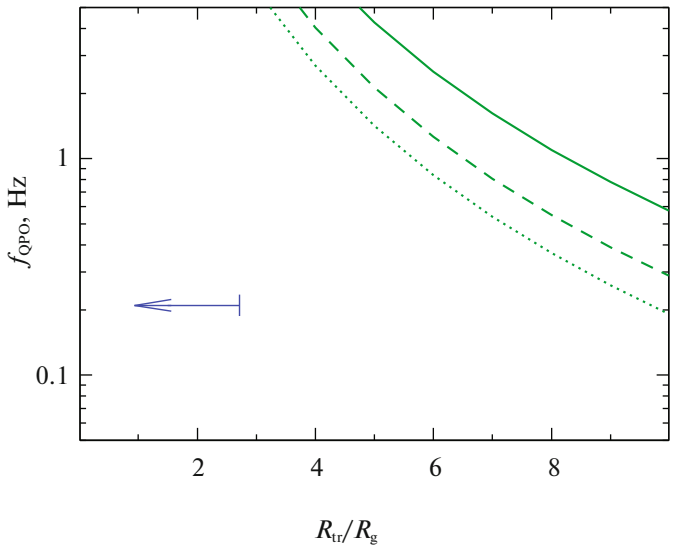


**Fig. 7.** (Color online) LF QPO frequency versus truncation radius according to the Lense–Thirring model (Ingram et al. 2014) for different black hole masses 10, 20, and 30 $M_\odot$ (the solid, dashed, and dotted lines, respectively). The black hole spin is taken to be 0.84 (the lower limit obtained by Xu et al. (2017) from the NuSTAR satellite data near MJD 58 004.3). The arrow indicates the maximum truncation radius from the NuSTAR data, the QPO frequency was measured based on the simultaneous XRT/SWIFT observations.

the Keplerian frequency is much higher than the measured QPO frequency. The only known QPO model that could give a reasonable QPO frequency in this case is the model by Ingram et al. (2009, 2014) for the formation of QPOs through the Lense–Thirring precession of the inner hot disk region. According to Ingram et al. (2014), depending on the black hole mass $M$ and spin $a$, the QPO frequency is defined by the formula

$$\frac{f_{\rm QPO}}{f_{\rm K}^*} = \left(1 - \sqrt{1 - \sqrt{2}ar^{3/2} + 0.75a^2r^2}\right),$$

where $r = R_{\rm g}/R_{\rm tr}$ and the relativistic Keplerian frequency

$$f_{\rm K}^* = \left(\frac{c}{\pi R_{\rm g}}\right)\left[\left(\frac{2}{r}\right)^{3/2} + a\right]^{-1}.$$

The predictions of the Lense–Thirring model calculated with this formula for a black hole with a mass of 10, 20, and even 30 $M_\odot$, which are presented in Fig. 7, differ greatly from the observations. This contradiction can arise both from the incorrect interpretation of the spectra and from the inconsistency of the QPO generation mechanism with the proposed one.

## *APPENDIX*

## EXTRACTION OF THE BAT/SWIFT SPECTRA

The BAT/SWIFT telescope can operate in several different modes; some modes can be used simultaneously. The survey mode is used in most observations: in this mode the telescope is pointed at the chosen object, while the data acquisition system writes the distribution of recorded photons in energy for each detector pixel over the entire exposure time (usually from 500 to 1500 s). Since BAT/SWIFT at each instant sees approximately one sixth of the sky, using the survey data allows the spectra of many bright ($\gtrsim$100 mCrab in the 15–150 keV band) sources to be regularly obtained. We used the following data processing procedure.

(1) For each such histogram we selected the working and healthy detector pixels (`batdetmask`, here and below, the commands from the `Heasoft` package are given in parentheses). Then, we constructed an image of the detector plane (`batbinevt`) and searched for "hot" pixels (`bathotpix`).

(2) We constructed an image of the detector plane (`batbinevt`) once again, eliminating the previously found nonworking or hot pixels. A sky image and a partial coding map were constructed (`batfftimage`). Sources were recorded in the sky image (`batcelldetect`).

(3) If a source was recorded at a statistically significant level, then the input data were subjected to a more accurate recalibration (`baterebin`). We constructed a model shadow image of the source in the detector plane (`batmaskwtimg`) and extracted its spectrum (`batbinevt`).

(4) The spectrum was corrected by taking into account the ray-tracing results (`batupdatephakw`). The

errors of the fluxes in the energy channels were increased by taking into account the experimentally determined systematic errors (`batphasyserr`); the telescope response matrix was calculated (`batdrmgen`).

The spectra obtained in this way were used to construct the source's broadband spectra.

## ACKNOWLEDGMENTS

This work is based on the data from the INTEGRAL observatory retrieved via its Russian and European Science Data Centers, the SWIFT observatory retrieved via NASA/HEASARC, and the MAXI experiment onboard the International Space Station (ISS) retrieved via the site *maxi.riken.jp/top*. We are grateful to the Russian Foundation for Basic Research (project no. 17-02-01079-a), the program of the President of the Russian Federation for support of leading scientific schools (project no. NSh-10222.2016.2), and the "Transitional and Explosive Processes in Astrophysics" subprogram of program P-7 of the Presidium of the Russian Academy of Sciences for the financial support.

## REFERENCES

1. R. Bandyopadhyay, T. Shahbaz, P. A. Charles, M. H. van Kerkwijk, and T. Naylor, Mon. Not. R. Astron. Soc. **285**, 718 (1997).
2. S. D. Barthelmy, L. M. Barbier, J. R. Cummings, E. E. Fenimore, N. Gehrels, D. Hullinger, H. A. Krimm, C. B. Markwardt, et al., Space Sci. Rev. **120**, 143 (2005).
3. T. M. Belloni, Lect. Notes Phys. **53**, 794 (2010).
4. C. T. Britt, A. Bahramian, and J. Strader, Astron. Telegram **10816**, 1 (2017).
5. D. N. Burrows, J. E. Hill, J. A. Nousek, J. A. Kennea, A. Wells, J. P. Osborne, A. F. Abbey, A. Beardmore, et al., Space Sci. Rev. **120**, 165 (2005).
6. A. M. Cherepashchuk, *Close Binary Stars* (Fizmatlit, Moscow, 2013) [in Russian].
7. T. Dincer, Astron. Telegram **10716**, 1 (2017).
8. K. Ebisawa, K. Mitsuda, and H. Inoue, Publ. Astron. Soc. **41**, 519 (1989).
9. F. Fürst, M. A. Nowak, J. A. Tomsick, J. M. Miller, S. Corbel, M. Bachetti, S. E. Boggs, F. E. Christensen, et al., Astrophys. J. **808**, 122 (2015).
10. N. Gehrels, G. Chincarini, P. Giommi, K. O. Mason, J. A. Nousek, A. A. Wells, N. E. White, S. D. Barthelmy, et al., Astrophys. J. **611**, 1005 (2004).
11. S. A. Grebenev, R. A. Syunyaev, M. N. Pavlinskii, and I. A. Dekhanov, Astron. Lett. **17**, 413 (1991).
12. S. Grebenev, R. Sunyaev, M. Pavlinsky, E. Churazov, M. Gilfanov, A. Dyachkov, N. Khavenson, K. Sukhanov, et al., Astron. Astrophys. Suppl. Ser. **97**, 281 (1993).
13. S. A. Grebenev, R. A. Sunyaev, and M. N. Pavlinsky, Adv. Space Res. **19**, 15 (1997).
14. A. Ingram and S. Motta, Mon. Not. R. Astron. Soc. **444**, 2065 (2014).
15. A. Ingram, C. Done, and P. C. Fragile, Mon. Not. R. Astron. Soc. **397**, L101 (2009).
16. J. A. Kennea, Astron. Telegram **10731**, 1 (2017).
17. J. A. Kennea, P. A. Evans, A. P. Beardmore, H. A. Krimm, P. Romano, K. Yamaoka, M. Serino, and H. Negoro, Astron. Telegram **10700**, 1 (2017).
18. F. Lebrun, J. P. Leray, P. Lavocat, J. Crétolle, M. Arques, C. Blondél, C. Bonnin, A. Bouére, et al., Astron. Astrophys. **411**, L141 (2003).
19. N. Lund, C. Budtz-Jórgensen, N. J. Westergaard, S. Brandt, I. L. Rasmussen, A. Hornstrup, C. A. Oxborrow, J. Chenevez, et al., Astron. Astrophys. **411**, L231 (2003).
20. C. B. Markwardt, D. N. Burrows, J. R. Cummings, J. A. Kennea, F. E. Marshall, K. L. Page, D. M. Palmer, and M. H. Siegel, GCN Circ. **21788**, 1 (2017).
21. M. Matsuoka, K. Kawasaki, S. Ueno, H. Tomida, M. Kohama, M. Suzuki, Y. Adachi, M. Ishikawa, et al., Publ. Astron. Soc. **61**, 999 (2009).
22. I. A. Mereminskiy and S. A. Grebenev, Astron. Telegram **10734**, 1 (2017).
23. T. Mihara, M. Nakajima, M. Sugizaki, M. Serino, M. Matsuoka, M. Kohama, K. Kawasaki, H. Tomida, S. Ueno, and N. Kawai, Publ. Astron. Soc. **63**, S623 (2011).
24. J. M. Miller, J. Homan, and G. Miniutti, Astrophys. J. **652**, L113 (2006a).
25. J. M. Miller, J. Homan, D. Steeghs, M. Rupen, R. W. Hunstead, R. Wijnands, P. A. Charles, and A. C. Fabian, Astrophys. J. **653**, 525 (2006b).
26. J. M. Miller, J. A. Tomsick, M. Bachetti, D. Wilkins, S. E. Boggs, F. E. Christensen, W. W. Craig, A. C. Fabian, et al., Astrophys. J. **799**, L6 (2015).
27. S. Nakahira, H. Negoro, T. Mihara, W. Iwakiri, M. Sugizaki, M. Shidatsu, M. Matsuoka, S. Ueno, et al., Astron. Telegram **10729**, 1 (2017).
28. H. Negoro, M. Ishikawa, S. Ueno, H. Tomida, Y. Sugawara, N. Isobe, R. Shimomukai, T. Mihara, et al., Astron. Telegram **10699**, 1 (2017).
29. A. V. Prosvetov and S. A. Grebenev, Astron. Lett. **41**, 549 (2015).
30. R. C. Reis, J. M. Miller, A. C. Fabian, E. M. Cackett, D. Maitra, C. S. Reynolds, M. Rupen, D. T. H. Steeghs, R. Wijnands, Mon. Not. R. Astron. Soc. **410**, 2497 (2011).
31. R. A. Remillard and J. E. McClintock, Ann. Rev. Astron. Astrophys. **44**, 49 (2006).
32. T. D. Russell, J. C. A. Miller-Jones, G. R. Sivakoff, and A. J. Tetarenko (Jacpot Xrb Collab.), Astron. Telegram **10711**, 1 (2017).
33. S. Scaringi (ASTR211 Students), Astron. Telegram **10702**, 1 (2017).
34. N. I. Shakura and R. A. Sunyaev, Astron. Astrophys. **24**, 337 (1973).
35. G. J. Sobczak, J. E. McClintock, R. A. Remillard, W. Cui, A. M. Levine, E. H. Morgan, J. A. Orosz, and C. D. Bailyn, Astrophys. J. **531**, 537 (2000).
36. L. Stella and M. Vietri, Astrophys. J. **492**, L59 (1998).

37. R. A. Sunyaev and L. G. Titarchuk, Astron. Astrophys. **86**, 121 (1980).
38. R. A. Syunyaev, I. Yu. Lapshov, S. A. Grebenev, V. V. Efremov, A. S. Kaniovskii, D. K. Stepanov, S. N. Yunin, E. A. Gavrilova, et al., Sov. Astron. Lett. **14**, 327 (1988).
39. R. Syunyaev, V. Aref'ev, K. Borozdin, M. Gil'fanov, V. Efremov, A. Kaniovskii, E. Churazov, E. Kendziora, et al., Sov. Astron. Lett. **17**, 413 (1991).
40. Y. Tanaka and N. Shibazaki, Ann. Rev. Astron. Astrophys. **34**, 607 (1996).
41. A. J. Tetarenko, T. D. Russell, J. C. A. Miller-Jones, and G. R. Sivakoff (Jacpot Xrb Collab.), Astron. Telegram **10745**, 1 (2017).
42. L. Titarchuk, N. Shaposhnikov, and V. Arefiev, Astrophys. J. **660**, 556 (2007).
43. P. Ubertini, F. Lebrun, G. di Cocco, A. Bazzano, A. J. Bird, K. Broenstad, A. Goldwurm, G. la Rosa, et al., Astron. Astrophys. **411**, L131 (2003).
44. F. Vignarca, S. Migliari, T. Belloni, D. Psaltis, and M. van der Klis, Astron. Astrophys. **397**, 729 (2003).
45. A. Vikhlinin, E. Churazov, and M. Gilfanov, Astron. Astrophys. **287**, 73 (1994).
46. R. Wijnands and M. van der Klis, Astrophys. J. **514**, 939 (1999).
47. C. Winkler, T. J. L. Courvoisier, G. di Cocco, N. Gehrels, A. Giménez, S. Grebenev, W. Hermsen, J. M. Mas-Hesse, et al., Astron. Astrophys. **411**, L1 (2003).
48. Y. Xu, F. A. Harrison, J. A. Garcia, A. C. Fabian, F. Fürst, P. Gandhi, B. W. Grefenstette, J. M. Miller, J. A. Tomsick, and D. J. Walton, arXiv:1711.01346 (2017).

*Translated by V. Astakhov*